CHIN. PHYS. LETT. Vol. 38, No. 9 (2021) 094203

High-Fidelity Geometric Gates with Single Ions Doped in Crystals

Ao-Lin Guo(郭奥林), Tao Tu(涂涛)*, Le-Tian Zhu(朱乐天), and Chuan-Feng Li(李传锋)*

Key Laboratory of Quantum Information, University of Science and Technology of China, Chinese Academy of Sciences, Hefei 230026, China

(Received 30 June 2021; accepted 30 July 2021; published online 2 September 2021)

Single rare-earth ions doped in solids are one kind of the promising candidates for quantum nodes towards a scalable quantum network. Realizing a universal set of high-fidelity gate operations is a central requirement for functional quantum nodes. Here we propose geometric gate operations using the hybridized states of electron spin and nuclear spin of an ion embedded in a crystal. The fidelities of these geometric gates achieve 0.98 in the realistic experimental situations. We also show the robustness of geometric gates to pulse fluctuations and to environment decoherence. These results provide insights for geometric phases in dissipative systems and show a potential application of high fidelity manipulations for future quantum internet nodes.

DOI: 10.1088/0256-307X/38/9/094203

Quantum networks have important applications in various quantum information processing, from distributed quantum computing, long-distance quantum communication, to non-local quantum sensing.[1−4] The implementation of such networks requires functional quantum nodes with an ability to store and process quantum information. On the one hand, the nodes can interface to optical photons with high efficiency and store quantum information with long coherence times. On the other hand, the nodes can process quantum information with high fidelity in the presence of practical imperfections. A variety of physical systems have been demonstrated as platforms for quantum nodes, such as single ions trapped in electric fields,[5] single atoms in cavities,[6,7] electron spins in quantum dots,[8,9] and defects in diamond or silicon carbide.[10−14] Single rare-earth ions doped in crystals are a promising candidate for quantum nodes since they exhibit high coherence optical and spin transitions. Recently, there have been many significant advances in this unique system, such as individual ions being isolated[15,16] and coupled to nanocavities,[17,18] as well as realizing long spin coherence times and single-shot readout of spin states.[19] While these progresses have demonstrated that single ions in crystals are suited to quantum storage, achieving a high fidelity gate operation of spin states of single ions and combining them to realize a full-featured node remains an outstanding challenge.

The rare-earth ions doped in crystals have a complex hyperfine structure, which are sensitive to magnetic fluctuations from neighboring electron spins and nuclear spins. Furthermore, the ions are sensitive to electric field fluctuations that cause optical decoherence. Building functional quantum nodes with single ions in solids requires high fidelity gate operations, motivating the development of manipulation methods to combat noise and decoherence. Geometric phases are not only a fundamental concept in quantum physics, but also are a powerful resource for achieving high fidelity quantum control due to their intrinsic tolerance to local fluctuations. By employing the cyclic evolution of quantum states in the Hilbert space, the geometric phases can be either Berry phases[20−22] or holonomies,[23,24] depending on the different energy level structures. Such geometric phases have been initially demonstrated in numerous systems.[25−33] However, the design of geometric gate operations for the unique level structures of rare-earth ions in crystals has remained elusive.

In this Letter, we propose a universal set of geometric gates with an ion embedded in a nanocrystal. We choose three hyperfine levels of a rare-earth ion doped in solid and implement two microwave fields to drive the transitions between the three levels. By working with tailored relative amplitude and phase of the two control fields, we can realize a geometric gate operation acting on the spin states in the Hilbert space. Using quantum process tomography, we calculate the fidelities of a set of universal gates that exceed 98% under realistic experimental conditions. In addition, we characterize how pulse imperfections and environment decoherence affect geometric gate operations, which have been rarely addressed in previous work.[34,35] In combination with an efficient interface to optical photons, these geometric gate op-

Supported by the National Natural Science Foundation of China (Grant No. 11974336), and the National Key Research and Development Program of China (Grant No. 2017YFA0304100).
*Corresponding authors. Email: tutao@ustc.edu.cn; licf@ustc.edu.cn
© 2021 Chinese Physical Society and IOP Publishing Ltd

erations suggest that single rare-earth ions in crystals can be a competitive platform for full-functional quantum nodes.

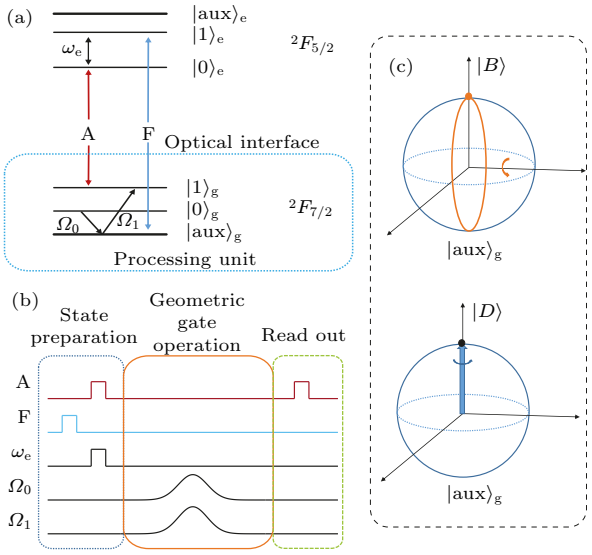

Fig. 1. (a) The energy level structure of a single ion $^{171}Yb^{3+}$ doped in a YVO_4 crystal. The spin states $|0\rangle_g$, $|1\rangle_g$ and $|\text{aux}\rangle_g$ form the processing unit for quantum nodes, while the excited states form the optical interface of the quantum nodes. (b) Pulse sequences for initialization, geometric gate operation and the readout of the spin states, enabling the functional quantum nodes. The geometric gates are realized by the simultaneous implementation of two pulses Ω_1 and Ω_2 with tailored pulse envelopes. (c) The geometric picture of the system dynamics under a cyclic evolution. The bright state $|B\rangle$ undergoes a rotation around the Y axis of the Bloch sphere, while the dark state $|D\rangle$ undergoes a trivial rotation around the north pole of the Bloch sphere. Thus the two states acquire the geometric phases $\gamma = \pi$ and $\gamma = 0$, respectively, proportional to the respective closed solid angles.

Rare-earth ions doped in crystals have emerged as promising candidates for quantum node platforms. Here we consider a typical system: a single ion $^{171}Yb^{3+}$ doped in a YVO_4 crystal.[19] The energy-level structure of this rare-earth ion system is illustrated in Figs. 1(a) and 1(b). The optical transitions between the ground state $^2F_{7/2}$ and the excited state $^2F_{5/2}$ form the interface with optical photons, which can be used to initialize and readout the spin states. The hyperfine interaction splits the ground state into three coupled electron–nuclear spin states: $|0\rangle_g = \frac{1}{\sqrt{2}}|\downarrow_e\Uparrow_n\rangle - |\uparrow_e\Downarrow_n\rangle$, $|1\rangle_g = \frac{1}{\sqrt{2}}|\downarrow_e\Uparrow_n\rangle + |\uparrow_e\Downarrow_n\rangle$ and $|\text{aux}\rangle_g = |\uparrow_e\Uparrow_n\rangle, |\downarrow_e\Downarrow_n\rangle$. Here we use the subscripts e, n to denote the electron spin $S = \frac{1}{2}$ and the nuclear spin $I = \frac{1}{2}$, respectively. The spin states $|0\rangle_g$ and $|1\rangle_g$ form the storage and processing unit of this solid-state quantum node. The states $|0\rangle_g$ and $|1\rangle_g$ have zero total spin, so these two states are first-order insensitive to external magnetic fluctuations, which results in a long spin coherence time. The spin transitions between $|0\rangle_g$, $|1\rangle_g$ and $|\text{aux}\rangle_g$ are in the microwave domain, which enables manipulations of these spin states with microwave fields.

The geometric gate operations for this unique system are designed as follows. We connect the $|0\rangle_g$ and $|1\rangle_g$ states to the auxiliary state $|\text{aux}\rangle_g$ via two tunable microwave fields $\Omega_0(t)$ and $\Omega_1(t)$. The two control fields have amplitudes as $\Omega_0(t) = \Omega(t)\cos\frac{\theta}{2}$ and $\Omega_1(t) = \Omega(t)\sin\frac{\theta}{2}e^{i\varphi}$, where $\Omega(t)$ describes the time-dependent pulse envelope, θ and φ describe the relative amplitude and phase between the two control fields. This three-level system has a bright state $|B\rangle = \cos\frac{\theta}{2}|0\rangle + \sin\frac{\theta}{2}e^{i\varphi}|1\rangle$ that undergoes populations to the auxiliary state, and a dark state $|D\rangle = -\sin\frac{\theta}{2}e^{-i\varphi}|0\rangle + \cos\frac{\theta}{2}|1\rangle$ that is decoupled from the dynamics. When $\Omega(t)$ has a cyclic evolution with $\Omega(0) = \Omega(\tau)$, the bright state and the dark state have different dynamics. As shown in Fig. 1(c), the bright state evolves as $|B(t)\rangle = e^{i\alpha}[\cos\alpha|B\rangle + \sin\alpha|\text{aux}\rangle_g]$ with $\alpha = \int\Omega(t)dt$. Thus, the bright state undergoes a rotation around the Y axis on the Bloch sphere spanned by the states $|B\rangle$ and $|\text{aux}\rangle_g$, acquiring a geometric phase $\gamma = \pi$. However, the dark state remains unchanged as $|D(t)\rangle = |D\rangle$. Thus the dark state undergoes trival dynamics around the north pole on the Bloch sphere spanned by the states $|D\rangle$ and $|\text{aux}\rangle_g$, acquiring a zero geometric phase $\gamma = 0$.

In the moving frame defined as $|m_0(t)\rangle = \cos\frac{\theta}{2}|B(t)\rangle - \sin\frac{\theta}{2}e^{i\varphi}|D(t)\rangle$, $|m_1(t)\rangle = \sin\frac{\theta}{2}e^{-i\varphi}|B(t)\rangle + \cos\frac{\theta}{2}|D(t)\rangle$, the system undergoes a cyclic evolution which satisfies the parallel-transport condition $\langle m_0(t)|H|m_1(t)\rangle = \langle m_1(t)|H|m_0(t)\rangle = 0$ ensuring the absence of a dynamic phase. Thus the system undergoes a cyclic evolution with the purely geometric contribution, and the cyclic evolution operator can be expressed as a transformation matrix in the computational basis of $|0\rangle_g$ and $|1\rangle_g$:

$$U(\theta,\varphi) = \begin{pmatrix} \cos\theta & \sin\theta e^{i\varphi} \\ \sin\theta e^{-i\varphi} & -\cos\theta \end{pmatrix}. \tag{1}$$

This operator represents a universal gate operation in the computational subspace of $|0\rangle_g$ and $|1\rangle_g$.

To investigate performance of the geometric gate operation, we consider the system dynamics under realistic situations. In the rotating frame, the Hamiltonian describing the two control fields within the rare-earth ion level structure is given by

$$H(t) = \begin{pmatrix} 0 & 0 & \Omega_0(t) \\ 0 & 0 & \Omega_1(t) \\ \Omega_0(t) & \Omega_1(t) & \Delta \end{pmatrix}, \tag{2}$$

on the bases of $|0\rangle_g$, $|1\rangle_g$, and $|\text{aux}\rangle_g$. In our simulations, the microwave pulses $\Omega_0(t) = \Omega(t)\cos\frac{\theta}{2}$ and $\Omega_1(t) = \Omega(t)\sin\frac{\theta}{2}e^{i\varphi}$ have a Gaussian pulse envelope $\Omega(t)$ with a maximum pulse amplitude of Ω_m and a total pulse duration of τ. Here we choose the pulse frequency detuning as $\Delta = 0$. The master equation in

the Lindblad form is given by

$$\frac{d\rho}{dt} = -i[\rho, H] + \sum_k \frac{1}{T_k} L_k[\rho], \tag{3}$$

where the Lindblad operators $L_k[\rho] = L_k \rho L_k^+ - \frac{1}{2} L_k^+ L_k \rho - \frac{1}{2} \rho L_k^+ L_k$ describe various dissipative processes. On the bases of $|0\rangle_g$, $|1\rangle_g$, and $|\text{aux}\rangle_g$, the dissipative operators are expressed as

$$\sum_k \frac{1}{T_k} L_k[\rho] = -\begin{pmatrix} \frac{1}{T_1}\rho_{00} & \frac{1}{T_2}\rho_{01} & \frac{1}{2T_1}\rho_{0a} \\ \frac{1}{T_2}\rho_{01} & \frac{1}{T_1}\rho_{11} & \frac{1}{2T_1}\rho_{1a} \\ \frac{1}{2T_1}\rho_{a0} & \frac{1}{2T_1}\rho_{a1} & -\frac{1}{T_1}(\rho_{00}+\rho_{11}) \end{pmatrix}. \tag{4}$$

Here, the relaxation processes from $|0\rangle_g$ to $|\text{aux}\rangle_g$ and from $|1\rangle_g$ to $|\text{aux}\rangle_g$ both have a relaxation time of $T_1 = 1\,\text{ms}$, the dephasing process between $|0\rangle_g$ and $|1\rangle_g$ has a dephasing time of $T_2 = 8\,\mu\text{s}$. In addition, we consider the spectral diffusion of the spin states by modeling the fluctuations of the frequency detuning $\delta\Delta$ as a Gaussian distribution with a standard deviation $\sigma_\Delta = 0.2\,\text{MHz}$. These values are extracted from the experimental measurements of time-resolved spin properties in rare-earth ions doped in crystals.[19] Sampling a random value of the noise $\delta\Delta$, then we numerically solve the master Eq. (3). This calculation is repeated many times and then averaged to give the final result.[36]

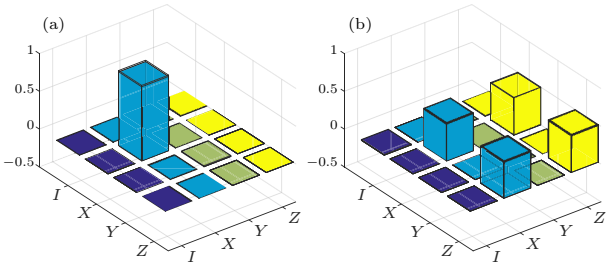

Fig. 2. The process tomography for the geometric X gate (a) and Hadmard gate (b). The bar charts show the simulated process matrix elements in the realistic situations. The wire frames show the ideal process matrix elements with the transformation Eq. (1). Here we fix the pulse amplitude $\Omega_m = 50\,\text{MHz}$.

We start from characterizing a set of universal gate operations. Different geometric gates can be achieved by choosing the corresponding pulse parameters θ and φ. Here we consider two widely used gate operations: an X gate with $\theta = \pi/2$ and $\varphi = 0$, a Hadmard gate with $\theta = \pi/4$ and $\varphi = 0$. We prepare the system in all three basis states, then calculate the dynamics of the system under the cyclic evolution, and measure it in all three bases. The results of the quantum process tomography are given in Fig. 2. As shown in Fig. 2, the matrix elements of the geometric gates are close to the matrix elements of ideal gates. More quantitatively, we define the fidelity of the gate operation as the overlap between the simulated process matrix χ_{sim} under realistic situations and the ideal process matrix χ_{ide}: $F = \text{Tr}(\chi_{\text{sim}}\chi_{\text{ide}})$. For the geometric X and Hadmard gates, we find the fidelities are $F_X = 0.981$ and $F_H = 0.982$, respectively. These fidelities are considerably higher than those ($\sim$0.86) reported so far for spin gate operations in the rare-earth ions system.[37] These results suggest that the gate operations based on geometric manipulations can achieve high fidelities even in realistic situations.

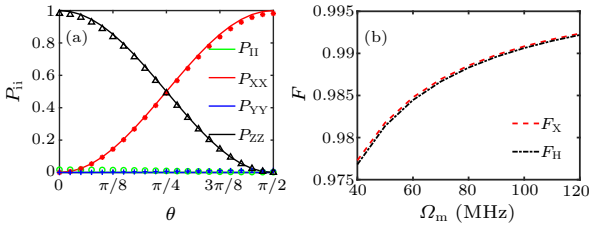

Fig. 3. (a) Diagonal elements of the process matrix as a function of the rotation angle θ of the pulse. The solid lines are calculated from Eq. (1). Here the pulse amplitude is fixed as $\Omega_m = 50\,\text{MHz}$. (b) The fidelity of the geometric gates as a function of the pulse amplitude Ω_m. Here F_X and F_H denote the fidelity of the geometric X and Hadmard gate, respectively.

We proceed to demonstrate universal gate operations by varying the rotation angle parameter θ of the pulse. With fixed $\varphi = 0$, we show the relationship between the diagonal elements of the process matrix and the θ degree of freedom in Fig. 3(a). As illustrated in the transformation Eq. (1), the geometric gate induces a rotation in the computational subspace as θ varies. The solid lines are given by the ideal transformation Eq. (1) without decoherence, while the dots are obtained from numerical simulations of the master equation including environment decoherence processes. Notably, the discrepancies between the realistic operation results and the ideal operation results are small. Next we examine the geometric gate operations for different pulse amplitudes Ω_m. The results are shown in Fig. 3(b). The fidelity of the geometric X gate and Hadmard gate increases as the pulse amplitude Ω_m increases. The main contribution to the gate error $1 - F$ comes from the environment decoherence during the cyclic evolution. Thus increasing the pulse amplitude Ω_m reduces the corresponding pulse duration τ, which in turn reduces the effect of decoherence. The fidelity increases beyond the threshold of 99% for fault-tolerant quantum computation[38,39] when the pulse amplitude exceeds 90 MHz.

To explicitly show the robustness of the geometric gates, we study the fidelities as a function of different pulse imperfections. As shown in Fig. 1(c), the geometric phase arises from the solid angle of the state evolution path, offering robustness to local fluctua-

tions along the path. In the simulations, we introduce two types of noises: the amplitude noise $\delta\Omega_{\rm m}$ around the amplitude parameter $\Omega_{\rm m}$, and the angle noise $\delta\theta$ around the rotation angle parameter θ. The two types of noises are assumed as a Gaussian distribution with a standard deviation $\sigma_{\Omega_{\rm m}}$ and σ_θ, respectively.[36] We calculate the average fidelity realized from many instances of noisy evolution paths. In Figs. 4(a) and 4(b), we examine the effect of the two different types of noises. In both the cases, the fidelity of geometric gates preserve a high value for larger noise strength. For example, when the deviation $\sigma_{\Omega_{\rm m}}$ of the pulse amplitude noise increases to 2.5 MHz, the fluctuation of the pulse amplitude is approximately 5% ($\frac{\sigma_{\Omega_{\rm m}}}{\Omega_{\rm m}}$), which is a considerable parameter fluctuation in typical experimental situations. We find that the fidelity of the geometric gates remains 0.97. This robustness feature results from the solid angle-preserving nature of the evolution path, where the geometric phase is not susceptible to fluctuations in the pulse parameters.

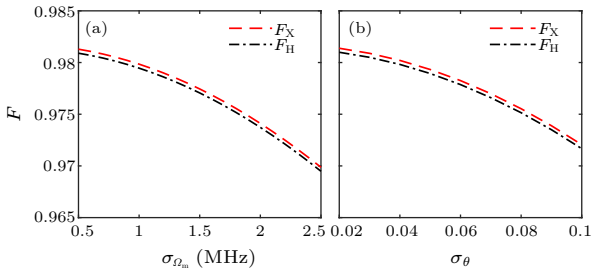

Fig. 4. The fidelity of the geometric gates as a function of the fluctuations in the pulse parameters: (a) the deviation $\sigma_{\Omega_{\rm m}}$ of the amplitude noise, (b) the deviation σ_θ of the rotation angle noise. Here the pulse amplitude is fixed as $\Omega_{\rm m} = 50$ MHz. $F_{\rm X}$ and $F_{\rm H}$ denote the fidelity of the geometric X and Hadmard gate, respectively.

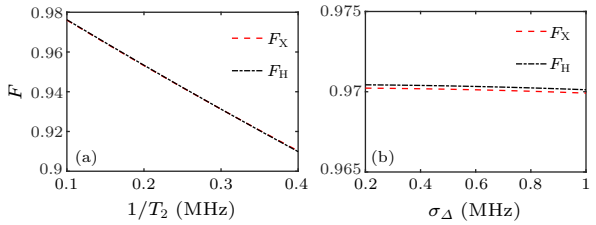

Fig. 5. The fidelity of the geometric gates as a function of the environment decoherence process: (a) the spin dephasing rate $1/T_2$, (b) the deviation σ_Δ of the spectral diffusion. Here the pulse amplitude is fixed as $\Omega_{\rm m} = 50$ MHz. $F_{\rm X}$ and $F_{\rm H}$ denote the fidelity of the geometric X and Hadmard gate, respectively.

Furthermore, we investigate the robustness to the environment decoherence. Although the geometric phase is determined by the global properties of the evolution path, the dynamics of the system is exposed to the decoherence effects of the environment. Since the relaxation process only affects the populations of the spin states, its effect on the system dynamics is minor. However, the dephasing process and the spectral diffusion mechanism affect the phase accumulation of the system. In Figs. 5(a) and 5(b), we plot the fidelity dependence on the dephasing time T_2 and on the spectral diffusion strength σ_Δ. For example, when the dephasing time T_2 is reduced to 2.5 μs, which is a typically small coherence time for solid-state spin systems, the geometric gate fidelity remains 0.92. In addition, the fidelity is more resilient to the spectral diffusion strength σ_Δ as shown in Fig. 5(b). Thus the geometric gates are robust to environment decoherence processes such as the dephasing and the spectral diffusion.

Finally, we extend the above scheme to realize a two-qubit gate. We choose two neighboring ions as the control and target qubits, respectively. The two ion spins are interacting through dipole couplings. Thus, the relevant two-spin space is spanned by the basis states of $|0_{\rm c}, 0_{\rm t}\rangle$, $|0_{\rm c}, 1_{\rm t}\rangle$, $|0_{\rm c}, {\rm aux}_{\rm t}\rangle$, $|1_{\rm c}, 0_{\rm t}\rangle$, $|1_{\rm c}, 1_{\rm t}\rangle$, $|1_{\rm c}, {\rm aux}_{\rm t}\rangle$. Here the subscripts c and t indicate the control and target qubits, respectively. We apply two tunable microwave fields $\Omega_0(t)$ and $\Omega_1(t)$ to couple the basis states $|0_{\rm c}, 0_{\rm t}\rangle$, $|0_{\rm c}, {\rm aux}_{\rm t}\rangle$, and $|0_{\rm c}, 1_{\rm t}\rangle$, $|0_{\rm c}, {\rm aux}_{\rm t}\rangle$, respectively. Therefore, we have the coupling Hamiltonian

$$H_2 = \frac{1}{\sqrt{2}}\left[(\Omega_0|0_{\rm c}, 0_{\rm t}\rangle + \Omega_1|0_{\rm c}, 1_{\rm t}\rangle)\langle 0_{\rm c}, {\rm aux}_{\rm t}| + {\rm H.c.}\right]. \tag{5}$$

We note that the two-qubit Hamiltonian has a form similar to that of the single-qubit Hamiltonian (2). We fix the ratio $\Omega_0/\Omega_1 = -1$. Under a cyclic evolution, this geometric process generates an operator in the two-qubit space

$$U_2 = |0_{\rm c}\rangle\langle 0_{\rm c}| \otimes X + |1_{\rm c}\rangle\langle 1_{\rm c}| \otimes I. \tag{6}$$

Here X and I denote the Pauli matrix σ_x and unit matrix on the target qubit. In this way, we can realize a geometric two-qubit CNOT gate.

In summary, we have proposed a universal set of geometric gate operations using a single rare-earth ion doped in a crystal. The optical transitions of the ion can form an efficient interface for quantum nodes, and the spin transitions of the ion can be used to implement manipulation and processing functions of quantum nodes. Here we use two microwave fields to drive three spin states undergoing cyclic evolution on the Bloch sphere to accumulate a geometric phase. We investigate the fidelity of this geometric gate in realistic experimental situations, as well as its robustness to fluctuations in the control parameters and various decoherence processes. Thus the geometric gates of spin states of ions become a necessary ingredient of function nodes. Combined with photon transfer, these geometric gate operations can be used to enable geometric quantum computation on a quantum network, a promising way of distributed

quantum computing.[38,39] The scheme can be designed for other scalable rare-earth ion systems with ultra-long spin coherence times or telecommunication-wavelength interfaces, such as Eu, Pr and Er ions doped in crystals.[40−44]

References

[1] Kimble H J 2008 *Nature* **453** 1023
[2] Sangouard N, Simon C, de Riedmatten H and Gisin N 2011 *Rev. Mod. Phys.* **83** 33
[3] Northup T E and Blatt R 2014 *Nat. Photon.* **8** 356
[4] Wehner1 S, Elkouss D and Hanson R 2018 *Science* **362** eaam9288
[5] Duan L M and Monroe C 2010 *Rev. Mod. Phys.* **82** 1209
[6] Ritter S *et al.* 2012 *Nature* **484** 195
[7] Reiserer A and Rempe G 2015 *Rev. Mod. Phys.* **87** 1379
[8] Gao W B, Fallahi P, Togan E, Miguel-Sanchez J and Imamoglu A 2012 *Nature* **491** 426
[9] De Greve K *et al.* 2012 *Nature* **491** 421
[10] Bernien H *et al.* 2013 *Nature* **497** 86
[11] Koehl W F, Buckley B B, Heremans F J, Calusine G and Awschalom D D 2011 *Nature* **479** 84
[12] Sipahigil A *et al.* 2016 *Science* **354** 847
[13] Nguyen C T *et al.* 2019 *Phys. Rev. Lett.* **123** 183602
[14] Awschalom D D, Hanson R, Wrachtrup J and Zhou B B 2018 *Nat. Photon.* **12** 516
[15] Kolesov R *et al.* 2012 *Nat. Commun.* **3** 1029
[16] Utikal T *et al.* 2014 *Nat. Commun.* **5** 3627
[17] Zhong T *et al.* 2018 *Phys. Rev. Lett.* **121** 183603
[18] Dibos A M, Raha M, Phenicie C M and Thompson J D 2018 *Phys. Rev. Lett.* **120** 243601
[19] Kindem J M *et al.* 2020 *Nature* **580** 201
[20] Berry M V 1984 *Proc. R. Soc. A* **392** 45
[21] Aharonov Y and Anandan J 1987 *Phys. Rev. Lett.* **58** 1593
[22] Zhu S L and Wang Z D 2002 *Phys. Rev. Lett.* **89** 097902
[23] Wilczek F and Zee A 1984 *Phys. Rev. Lett.* **52** 2111
[24] Sjoqvist E, Tong D M, Andersson L M, Hessmo B, Johansson M and Singh K 2012 *New J. Phys.* **14** 103035
[25] Feng G, Xu G and Long G 2013 *Phys. Rev. Lett.* **110** 190501
[26] Abdumalikov A A, Fink J M, Juliusson K, Pechal M, Berger S, Wallraff A and Filipp S 2013 *Nature* **496** 482
[27] Zu C, Wang W B, He L, Zhang W G, Dai C Y, Wang F and Duan L M 2014 *Nature* **514** 72
[28] Zhou B B *et al.* 2017 *Phys. Rev. Lett.* **119** 140503
[29] Xu Y *et al.* 2018 *Phys. Rev. Lett.* **121** 110501
[30] Huang Y Y *et al.* 2019 *Phys. Rev. Lett.* **122** 010503
[31] Yan T X *et al.* 2019 *Phys. Rev. Lett.* **122** 080501
[32] Xu Y *et al.* 2020 *Phys. Rev. Lett.* **124** 230503
[33] Zhang W L *et al.* 2021 *Phys. Rev. Lett.* **127** 030502
[34] Solinas P, Zanardi P and Zangh N 2004 *Phys. Rev. A* **70** 042316
[35] Zhu S L and Zanardi P 2005 *Phys. Rev. A* **72** 020301
[36] Watson T F, Philips S G J, Kawakami E, Ward D R, Scarlino P, Veldhorst M, Savage D E, Lagally M G, Friesen M, Coppersmith S N, Eriksson M A and Vandersypen L M K 2018 *Nature* **555** 633
[37] Wolfowicz G, Maier-Flaig H, Marino R, Ferrier A, Vezin H, Morton J J L and Goldner P 2015 *Phys. Rev. Lett.* **114** 170503
[38] Nickerson N H, Li Y and Benjamin S C 2013 *Nat. Commun.* **4** 1756
[39] Nickerson N H, Fitzsimons J F and Benjamin S C 2014 *Phys. Rev. X* **4** 041041
[40] Gundogan M, Ledingham P M, Kutluer K, Mazzera M and de Riedmatten H 2015 *Phys. Rev. Lett.* **114** 230501
[41] Jobez P *et al.* 2015 *Phys. Rev. Lett.* **114** 230502
[42] Lauritzen B, M, J, de Riedmatten H, Afzelius M, Sangouard N, Simon C and Gisin N 2010 *Phys. Rev. Lett.* **104** 080502
[43] Zhou Z Q, Hua Y L, Liu X, Chen G, Xu J S, Han Y J, Li C F and Guo G C 2015 *Phys. Rev. Lett.* **115** 070502
[44] Gong B, Tu T, Guo A L, Zhu L T and Li C F 2021 *Chin. Phys. Lett.* **38** 044201